1 Comparing single- and multi-image NEB calculations

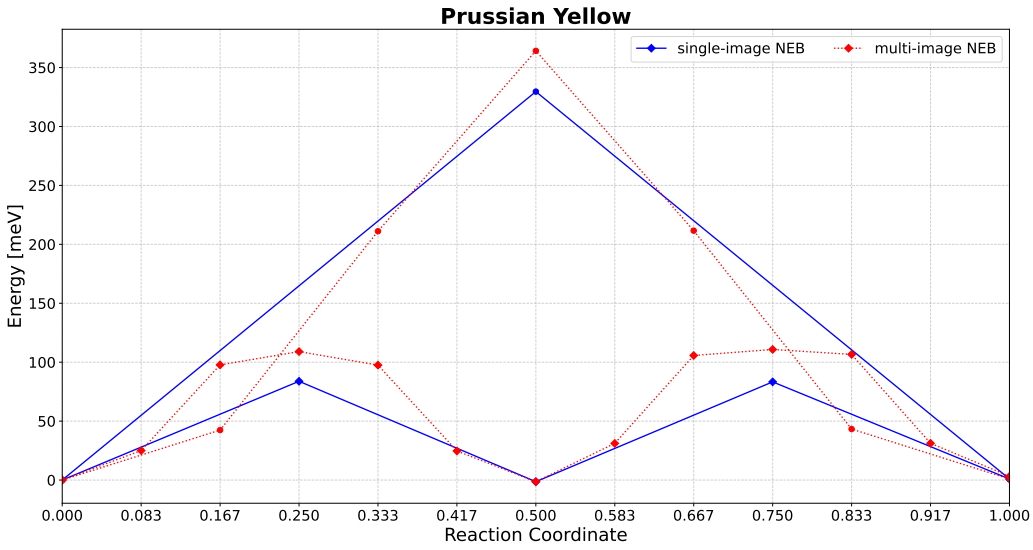

Figure S1: Plot of the calculated migration barrier for the cubic Prussian Yellow system. Shown are the ladder-like migration mechanism (diamonds) and the diffusion across the large central void (dots). The single-image NEB calculations are colored blue, while the multi-image NEB results are shown in red.

Figure S1 presents a side-by-side comparison of migration barriers obtained using the single-image and standard multi-image NEB approaches for the cubic modification of Prussian Yellow. This model system was selected because it contains only one migrating sodium ion and exhibits an unobstructed diffusion pathway, enabling a clean and direct methodological comparison. The two approaches yield closely aligned barriers, with deviations limited to 30 meV. Notably, the multi-image NEB produces marginally higher barriers, which we attribute to image crowding: using only five images along relatively short migration paths ($\sim$3 Å for the ladder mechanism and $\sim$5 Å for the void mechanism) can lead to artificial repulsion between adjacent images, subtly inflating the calculated transition state energy. These observations support the conclusion that the single-image NEB approach is well-suited for Prussian Blue systems and provides a computationally efficient

yet accurate representation of migration energetics.

2 Experimentally observed lattice constants[1]

The graph is included to support the observation made in the main text of a linear dependence between the lattice constant and the sodium content in Prussian Blue analogues. Experimental data, sourced from Ref.,[1] were linearly fitted and the resulting fit was extrapolated to a sodium content of two atoms per formula unit. The extrapolated endpoint was added for visual clarity and to enable a direct comparison with the values obtained from first-principles calculations in this work.

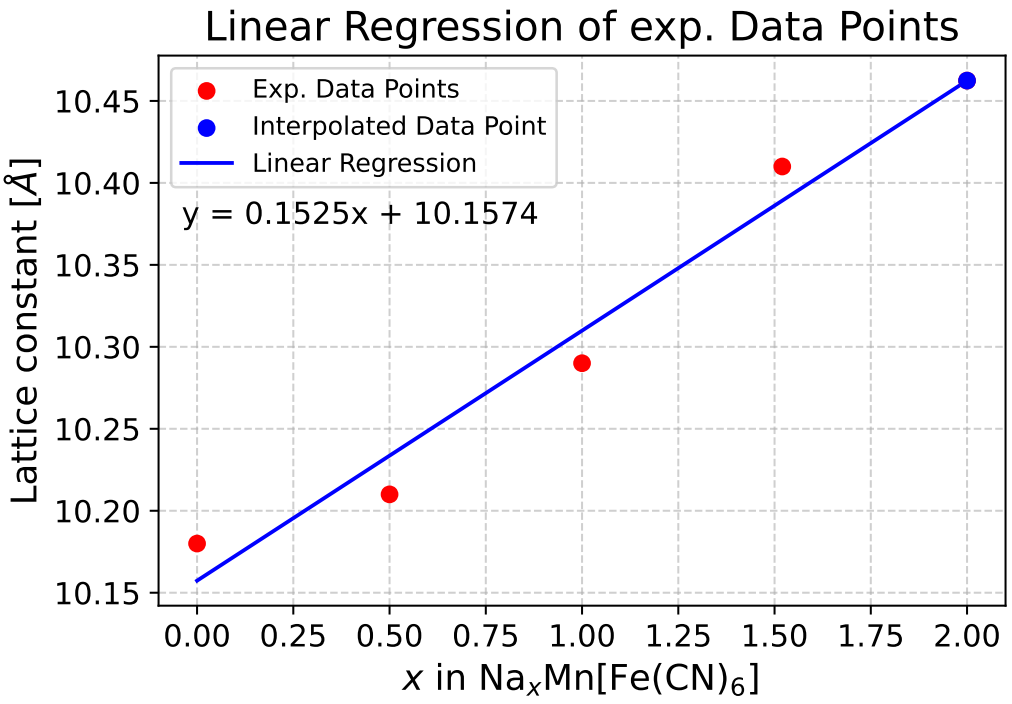

Figure S2: Lattice constant in dependence on the charging state of the Prussian blue cathode material as measured by in-situ XRD. Experimental values are taken from Wu et al.[1]

3 Sodium in the 8c Wyckoff position structures

In the following section, we present the model system of a cubic Prussian Blue structure, in which sodium atoms have been intercalated into the 8c Wyckoff position. These structures are visualized below in Figure S3. The calculated structural and electronic properties are presented in the subsections that follow.

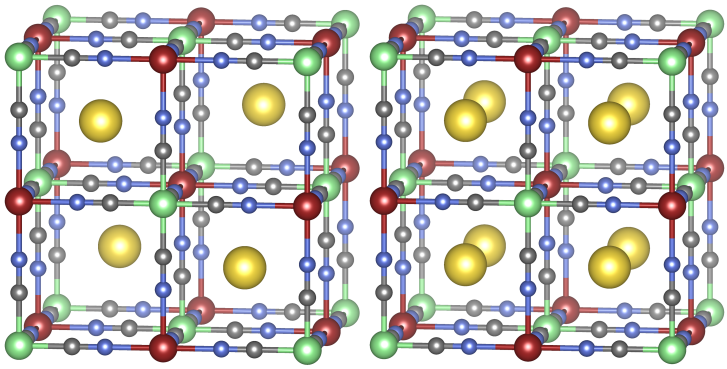

Figure S3: A depiction of the atomic structures within the unit cell of the cubic Prussian Blue (left) and cubic Prussian White (right), for the model case of sodium intercalating into the Wyckoff 8c position. High- and low-spin iron atoms are represented in red and green, respectively. Carbon atoms are shown in grey, nitrogen atoms in blue, and sodium atoms in yellow.

3.1 Cubic Prussian Blue

Tabulated data for the nonphysical model system of the cubic Prussian Blue ($Fm\bar{3}m$ / 225) structure with sodium being intercalated into the 8c position for all benchmarked functionals.

Table S1: Structural properties of the cubic Prussian Blue structure with sodium being intercalated into the 8c position.

Property	PBE	PBE+U	SCAN	r^{2}SCAN	PBE0	HSE06
a, b, c [Å]	10.233	10.259	10.152	10.168	10.164	10.168
V [Å^3]	1071.62	1079.76	1046.38	1051.38	1050.03	1051.14
d(Fe_{ls}^{2+}-C) [Å]	1.872	1.882	1.863	1.866	1.871	1.870
d(C-N) [Å]	1.177	1.176	1.167	1.170	1.164	1.165
d(Fe_{hs}^{2+}-N) [Å]	2.067	2.071	2.045	2.048	2.047	2.048
α(Fe_{ls}^{2+}-C-N) [°]	180	180	180	180	180	180
α(Fe_{hs}^{2+}-N-C) [°]	180	180	180	180	180	180
α(C-Fe_{ls}^{2+}-C) [°]	90	90	90	90	90	90
α(N-Fe_{hs}^{2+}-N) [°]	90	90	90	90	90	90

Table S2: Electronic properties of the cubic Prussian Blue structure with sodium being intercalated into the 8c position.

Property	PBE	PBE+U	SCAN	r^{2}SCAN	PBE0	HSE06
VB_{Max} [eV]	-0.371	-0.44	-0.41	-0.382	-1.412	-1.044
CB_{min} [eV]	0.196	1.373	0.525	0.475	1.497	1.139
ΔE_g [eV]	0.567	1.813	0.935	0.857	2.909	2.183
$\mu_{Fe(II)\text{-}C}$ [μ_B]	0.338	0.139	0.234	0.247	0.113	0.12
$\mu_{Fe(II)\text{-}N}$ [μ_B]	3.854	4.306	4.036	4.033	4.183	4.179

3.2 Cubic Prussian White

Tabulated data for the nonphysical model system of the cubic Prussian White ($Fm\bar{3}m$ / 225) structure with sodium being intercalated into the 8c position for all benchmarked functionals.

Table S3: Structural properties of the cubic Prussian Blue structure with sodium being intercalated into the 8c position.

Property	PBE	PBE+U	SCAN	r^{2}SCAN	PBE0	HSE06
a, b, c [Å]	10.308	10.349	10.239	10.249	10.327	10.329
V [Å^3]	1095.15	1108.43	1072.74	1076.59	1101.21	1102.11
d(Fe_{ls}^{2+}-C) [Å]	1.867	1.883	1.861	1.863	1.873	1.874
d(C-N) [Å]	1.181	1.181	1.171	1.174	1.166	1.166
d(Fe_{hs}^{2+}-N) [Å]	2.106	2.111	2.086	2.088	2.124	2.125
α(Fe_{ls}^{2+}-C-N) [°]	180	180	180	180	180	180
α(Fe_{hs}^{2+}-N-C) [°]	180	180	180	180	180	180
α(C-Fe_{ls}^{2+}-C) [°]	90	90	90	90	90	90
α(N-Fe_{hs}^{2+}-N) [°]	90	90	90	90	90	90

Table S4: Electronic properties of the cubic Prussian Blue structure with sodium being intercalated into the 8c position.

Property	PBE	PBE+U	SCAN	r^{2}SCAN	PBE0	HSE06
VB_{Max} [eV]	–	–	–	–	0.612	0.978
CB_{min} [eV]	–	–	–	–	3.580	3.243
ΔE_g [eV]	cond.	cond.	cond.	cond.	2.968	2.265
$\mu_{Fe(II)\text{-}C}$ [μ_B]	0.110	0.002	0.059	0.073	0.021	0.026
$\mu_{Fe(II)\text{-}N}$ [μ_B]	3.426	3.889	3.566	3.564	3.552	3.553

4 Floating point data on FeHCF

In all tables of this section, the lattice constant along the c-axis for cubic compounds is omitted for clarity as it is equal to the a- and b-axis value. In cases where structural distortions led to variations in the bond lengths within the octahedra, the individual bond lengths were averaged based on their stoichiometric ratios. This approach was adopted to present the data more clearly and to facilitate meaningful comparison across compounds.

4.1 PBE functional

Tabulated data for the FeHCF compound calculated with the PBE functional.

Table S5: Structural properties of Prussian Yellow (PY), Prussian Blue (PB), cubic Prussian White (PW) and rhombohedral Prussian White (RPW) as calculated with the PBE functional.

Property	PY	PB	PW	RPW
Space group	$Fm\bar{3}m$ (225)	$Fm\bar{3}m$ (225)	$Fm\bar{3}m$ (225)	$R\bar{3}$ (148)
a, b [Å]	10.260	10.267	10.400	6.432
c [Å]	–	–	–	19.206
V [Å^3]	1079.94	1082.36	1124.88	688.18
d(Fe_{ls}^{2+}-C) [Å]	1.895	1.879	1.881	1.872
d(C-N) [Å]	1.172	1.178	1.182	1.185
d(Fe_{hs}^{2+}-N) [Å]	2.063	2.078	2.138	2.155
α(Fe_{ls}^{2+}-C-N) [°]	180	180	180	172.2
α(Fe_{hs}^{2+}-N-C) [°]	180	180	180	141.9
α(C-Fe_{ls}^{2+}-C) [°]	90	90	90	86.7/93.3
α(N-Fe_{hs}^{2+}-N) [°]	90	90	90	91.1/88.9

Table S6: Electronic properties of Prussian Yellow (PY), Prussian Blue (PB), cubic Prussian White (PW) and rhombohedral Prussian White (RPW) as calculated with the PBE functional.

Property	PY	PB	PW	RPW
VB_{Max} [eV]	–	-0.636	1.365	–
CB_{min} [eV]	–	-0.21	1.784	–
ΔE_g [eV]	cond.	0.426	0.419	cond.
$\mu_{Fe(II)\text{-}C}$ [μ_B]	1.050	0.344	0.068	0.106
$\mu_{Fe(II)\text{-}N}$ [μ_B]	3.869	3.855	3.439	3.344

4.2 PBE+U functional

Tabulated data for the FeHCF compound calculated with the PBE+U (U=7/3) functional.

Table S7: Structural properties of Prussian Yellow (PY), Prussian Blue (PB), cubic Prussian White (PW) and rhombohedral Prussian White (RPW) as calculated with the PBE+U functional.

Property	PY	PB	PW	RPW
Space group	$Fm\bar{3}m$ (225)	$Fm\bar{3}m$ (225)	$Fm\bar{3}m$ (225)	$R\bar{3}$ (148)
a, b [Å]	10.297	10.296	10.521	6.480
c [Å]	–	–	–	19.364
V [Å^3]	1091.62	1091.58	1064.65	704.05
d(Fe_{ls}^{2+}-C) [Å]	1.904	1.889	1.895	1.886
d(C-N) [Å]	1.170	1.177	1.180	1.183
d(Fe_{hs}^{2+}-N) [Å]	2.074	2.083	2.187	2.186
α(Fe_{ls}^{2+}-C-N) [°]	180	180	180	171.9
α(Fe_{hs}^{2+}-N-C) [°]	180	180	180	141.9
α(C-Fe_{ls}^{2+}-C) [°]	90	90	90	86.6/93.4
α(N-Fe_{hs}^{2+}-N) [°]	90	90	90	91.2/88.8

Table S8: Electronic properties of Prussian Yellow (PY), Prussian Blue (PB), cubic Prussian White (PW) and rhombohedral Prussian White (RPW) as calculated with the PBE+U functional.

Property	PY	PB	PW	RPW
VB_{Max} [eV]	–	–	-0.143	–
CB_{min} [eV]	–	–	3.412	–
ΔE_g [eV]	cond.	cond.	3.555	cond.
$\mu_{Fe(II)\text{-}C}$ [μ_B]	1.095	0.140	0.022	0.056
$\mu_{Fe(II)\text{-}N}$ [μ_B]	4.284	4.308	3.653	3.691

4.3 SCAN functional

Tabulated data for the FeHCF compound calculated with the SCAN functional.

Table S9: Structural properties of Prussian Yellow (PY), Prussian Blue (PB), cubic Prussian White (PW) and rhombohedral Prussian White (RPW) as calculated with the SCAN functional.

Property	PY	PB	PW	RPW
Space group	$Fm\bar{3}m$ (225)	$Fm\bar{3}m$ (225)	$Fm\bar{3}m$ (225)	$R\bar{3}$ (148)
a, b [Å]	10.185	10.191	10.317	6.297
c [Å]	–	–	–	19.272
V [Å^3]	1056.44	1058.46	1098.22	661.84
d(Fe_{ls}^{2+}-C) [Å]	1.884	1.871	1.872	1.868
d(C-N) [Å]	1.162	1.168	1.171	1.175
d(Fe_{hs}^{2+}-N) [Å]	2.046	2.058	2.115	2.138
α(Fe_{ls}^{2+}-C-N) [°]	180	180	180	170.8
α(Fe_{hs}^{2+}-N-C) [°]	180	180	180	140.7
α(C-Fe_{ls}^{2+}-C) [°]	90	90	90	86.3/93.7
α(N-Fe_{hs}^{2+}-N) [°]	90	90	90	91.1/88.9

Table S10: Electronic properties of Prussian Yellow (PY), Prussian Blue (PB), cubic Prussian White (PW) and rhombohedral Prussian White (RPW) as calculated with the SCAN functional.

Property	PY	PB	PW	RPW
VB_{Max} [eV]	–	-0.705	0.990	–
CB_{min} [eV]	–	0.082	1.467	–
ΔE_g [eV]	cond.	0.787	2.457	cond.
$\mu_{Fe(II)\text{-}C}$ [μ_B]	1.058	0.236	0.036	0.078
$\mu_{Fe(II)\text{-}N}$ [μ_B]	4.030	4.039	3.537	3.459

4.4 r²SCAN functional

Tabulated data for the FeHCF compound calculated with the r²SCAN functional.

Table S11: Structural properties of Prussian Yellow (PY), Prussian Blue (PB), cubic Prussian White (PW) and rhombohedral Prussian White (RPW) as calculated with the r²SCAN functional.

Property	PY	PB	PW	RPW
Space group	$Fm\bar{3}m$ (225)	$Fm\bar{3}m$ (225)	$Fm\bar{3}m$ (225)	$R\bar{3}$ (148)
a, b [Å]	10.206	10.213	10.348	6.320
c [Å]	–	–	–	19.247
V [Å^3]	1063.13	1065.22	1108.09	665.82
d(Fe_{ls}^{2+}-C) [Å]	1.889	1.874	1.876	1.869
d(C-N) [Å]	1.164	1.171	1.174	1.177
d(Fe_{hs}^{2+}-N) [Å]	2.049	2.062	2.124	2.142
α(Fe_{ls}^{2+}-C-N) [°]	180	180	180	171.0
α(Fe_{hs}^{2+}-N-C) [°]	180	180	180	140.7
α(C-Fe_{ls}^{2+}-C) [°]	90	90	90	86.5/93.5
α(N-Fe_{hs}^{2+}-N) [°]	90	90	90	91.0/89.0

Table S12: Electronic properties of Prussian Yellow (PY), Prussian Blue (PB), cubic Prussian White (PW) and rhombohedral Prussian White (RPW) as calculated with the r²SCAN functional.

Property	PY	PB	PW	RPW
VB_{Max} [eV]	–	-0.645	1.426	–
CB_{min} [eV]	–	0.027	2.393	–
ΔE_g [eV]	cond.	0.672	0.967	cond.
$\mu_{Fe(II)\text{-}C}$ [μ_B]	1.074	0.254	0.040	0.083
$\mu_{Fe(II)\text{-}N}$ [μ_B]	4.030	4.035	3.541	3.459

4.5 PBE0 functional

Tabulated data for the FeHCF compound calculated with the PBE0 functional.

Table S13: Structural properties of Prussian Yellow (PY), Prussian Blue (PB), cubic Prussian White (PW) and rhombohedral Prussian White (RPW) as calculated with the PBE0 functional.

Property	PY	PB	PW	RPW
Space group	$Fm\bar{3}m$ (225)	$Fm\bar{3}m$ (225)	$Fm\bar{3}m$ (225)	$R\bar{3}$ (148)
a, b [Å]	10.232	10.206	10.423	6.499
c [Å]	–	–	–	18.584
V [Å^3]	1071.21	1062.93	1132.49	679.81
d(Fe_{ls}^{2+}-C) [Å]	1.909	1.880	1.889	1.877
d(C-N) [Å]	1.157	1.165	1.167	1.171
d(Fe_{hs}^{2+}-N) [Å]	2.051	2.059	2.155	2.171
α(Fe_{ls}^{2+}-C-N) [°]	180	180	180	174.6
α(Fe_{hs}^{2+}-N-C) [°]	180	180	180	139.1
α(C-Fe_{ls}^{2+}-C) [°]	90	90	90	88.5/91.5
α(N-Fe_{hs}^{2+}-N) [°]	90	90	90	91.7/88.3

Table S14: Electronic properties of Prussian Yellow (PY), Prussian Blue (PB), cubic Prussian White (PW) and rhombohedral Prussian White (RPW) as calculated with the PBE0 functional.

Property	PY	PB	PW	RPW
VB_{Max} [eV]	-3.301	-1.742	-0.324	0.637
CB_{min} [eV]	-0.55	1.046	3.834	4.979
ΔE_g [eV]	2.751	2.788	4.158	4.342
$\mu_{Fe(II)\text{-}C}$ [μ_B]	1.000	0.115	0.018	0.036
$\mu_{Fe(II)\text{-}N}$ [μ_B]	4.205	4.187	3.568	3.519

4.6 HSE06 functional

Tabulated data for the FeHCF compound calculated with the HSE06 functional.

Table S15: Structural properties of Prussian Yellow (PY), Prussian Blue (PB), cubic Prussian White (PW) and rhombohedral Prussian White (RPW) as calculated with the HSE06 functional.

Property	PY	PB	PW	RPW
Space group	$Fm\bar{3}m$ (225)	$Fm\bar{3}m$ (225)	$Fm\bar{3}m$ (225)	$R\bar{3}$ (148)
a, b [Å]	10.238	10.222	10.420	–
c [Å]	–	–	–	–
V [Å^3]	1073.16	1068.06	1131.51	–
d(Fe_{ls}^{2+}-C) [Å]	1.909	1.882	1.887	–
d(C-N) [Å]	1.157	1.166	1.167	–
d(Fe_{hs}^{2+}-N) [Å]	2.054	2.064	2.156	–
α(Fe_{ls}^{2+}-C-N) [°]	180	180	180	–
α(Fe_{hs}^{2+}-N-C) [°]	180	180	180	–
α(C-Fe_{ls}^{2+}-C) [°]	90	90	90	–/–
α(N-Fe_{hs}^{2+}-N) [°]	90	90	90	–/–

Table S16: Electronic properties of Prussian Yellow (PY), Prussian Blue (PB), cubic Prussian White (PW) and rhombohedral Prussian White (RPW) as calculated with the HSE06 functional.

Property	PY	PB	PW	RPW
VB_{Max} [eV]	-2.936	-1.398	0.098	–
CB_{min} [eV]	-1.119	0.629	3.458	–
ΔE_g [eV]	1.817	2.027	3.360	–
$\mu_{Fe(II)\text{-}C}$ [μ_B]	1.005	0.124	0.019	–
$\mu_{Fe(II)\text{-}N}$ [μ_B]	4.205	4.185	3.569	–

5 Floating point data on MnHCF

In all tables of this section, the lattice constant along the c-axis for cubic compounds is omitted for clarity as it is equal to the a- and b-axis value.

In cases where structural distortions led to variations in the bond lengths within the octahedra, the individual bond lengths were averaged based on their stoichiometric ratios. This approach was adopted to present the data more clearly and to facilitate meaningful comparison across compounds.

5.1 PBE functional

Tabulated data for the MnHCF compound calculated with the PBE functional.

Table S17: Structural properties of the manganese analogue Prussian Yellow (PY), Prussian Blue (PB), cubic Prussian White (PW) and rhombohedral Prussian White (RPW) as calculated with the PBE functional.

Property	PY	PB	PW	RPW
Space group	$Fm\bar{3}m$ (225)	$Fm\bar{3}m$ (225)	$Fm\bar{3}m$ (225)	$R\bar{3}$ (148)
a, b [Å]	10.332	10.120	10.550	6.526
c [Å]	9.943	–	–	19.158
V [Å^3]	1061.37	1061.05	1174.14	706.56
d(Fe_{ls}^{2+}-C) [Å]	1.890	1.881	1.877	1.873
d(C-N) [Å]	1.171	1.178	1.182	1.185
d(Fe_{hs}^{2+}-N) [Å]	1.975	2.042	2.216	2.224
α(Fe_{ls}^{2+}-C-N) [°]	180	180	180	173.4
α(Fe_{hs}^{2+}-N-C) [°]	180	180	180	139.3
α(C-Fe_{ls}^{2+}-C) [°]	90	90	90	87.2/92.8
α(N-Fe_{hs}^{2+}-N) [°]	90	90	90	91.9/88.1

Table S18: Electronic properties of the manganese analogue Prussian Yellow (PY), Prussian Blue (PB), cubic Prussian White (PW) and rhombohedral Prussian White (RPW) as calculated with the PBE functional.

Property	PY	PB	PW	RPW
VB_{Max} [eV]	–	-0.627	–	–
CB_{min} [eV]	–	-0.016	–	–
ΔE_g [eV]	cond.	0.611	cond.	cond.
$\mu_{Fe(II)\text{-}C}$ [μ_B]	0.971	0.190	0.075	0.074
$\mu_{Fe(II)\text{-}N}$ [μ_B]	3.481	3.481	4.440	4.411

5.2 PBE+U functional

Tabulated data for the MnHCF compound calculated with the PBE+U functional.

Table S19: Structural properties of the manganese analogue Prussian Yellow (PY), Prussian Blue (PB), cubic Prussian White (PW) and rhombohedral Prussian White (RPW) as calculated with the PBE+U functional.

Property	PY	PB	PW	RPW
Space group	$Fm\bar{3}m$ (225)	$Fm\bar{3}m$ (225)	$Fm\bar{3}m$ (225)	$R\bar{3}$ (148)
a, b [Å]	10.157	10.718	10.666	7.433
c [Å]	10.625	–	–	18.572
V [Å^3]	1096.10	1231.12	1213.33	888.62
d(Fe_{ls}^{2+}-C) [Å]	1.920	1.936	1.906	1.894
d(C-N) [Å]	1.170	1.172	1.179	1.179
d(Fe_{hs}^{2+}-N) [Å]	2.145	2.255	2.248	2.219
α(Fe_{ls}^{2+}-C-N) [°]	180	180	180	179.1
α(Fe_{hs}^{2+}-N-C) [°]	180	180	180	178.8
α(C-Fe_{ls}^{2+}-C) [°]	90	90	90	89.4/90.6
α(N-Fe_{hs}^{2+}-N) [°]	90	90	90	90.3/89.7

Table S20: Electronic properties of the manganese analogue Prussian Yellow (PY), Prussian Blue (PB), cubic Prussian White (PW) and rhombohedral Prussian White (RPW) as calculated with the PBE+U functional.

Property	PY	PB	PW	RPW
VB_{Max} [eV]	–	–	–	–
CB_{min} [eV]	–	–	–	–
ΔE_g [eV]	cond.	cond.	cond.	cond.
$\mu_{Fe(II)\text{-}C}$ [μ_B]	1.132	-0.985	0.042	0.045
$\mu_{Fe(II)\text{-}N}$ [μ_B]	3.828	4.656	4.65	4.638

5.3 SCAN functional

Tabulated data for the MnHCF compound calculated with the SCAN functional.

Table S21: Structural properties of the manganese analogue Prussian Yellow (PY), Prussian Blue (PB), cubic Prussian White (PW) and rhombohedral Prussian White (RPW) as calculated with the SCAN functional.

Property	PY	PB	PW	RPW
Space group	$Fm\bar{3}m$ (225)	$Fm\bar{3}m$ (225)	$Fm\bar{3}m$ (225)	$R\bar{3}$ (148)
a, b [Å]	10.304	10.145	10.478	6.393
c [Å]	9.893	–	–	19.149
V [Å^3]	1050.41	1044.00	1150.52	677.85
d(Fe_{ls}^{2+}-C) [Å]	1.890	1.877	1.867	1.869
d(C-N) [Å]	1.160	1.169	1.171	1.175
d(Fe_{hs}^{2+}-N) [Å]	1.965	2.027	2.201	2.209
α(Fe_{ls}^{2+}-C-N) [°]	180	180	180	172.5
α(Fe_{hs}^{2+}-N-C) [°]	180	180	180	137.6
α(C-Fe_{ls}^{2+}-C) [°]	90	90	90	87.2/92.8
α(N-Fe_{hs}^{2+}-N) [°]	90	90	90	91.8/88.2

Table S22: Electronic properties of the manganese analogue Prussian Yellow (PY), Prussian Blue (PB), cubic Prussian White (PW) and rhombohedral Prussian White (RPW) as calculated with the SCAN functional.

Property	PY	PB	PW	RPW
VB_{Max} [eV]	–	-0.689	-0.568	0.295
CB_{min} [eV]	–	-0.3	-0.094	0.792
ΔE_g [eV]	cond.	0.389	0.474	0.497
$\mu_{Fe(II)\text{-}C}$ [μ_B]	0.948	0.143	0.058	0.063
$\mu_{Fe(II)\text{-}N}$ [μ_B]	3.598	3.569	4.505	4.476

5.4 r^{2}SCAN functional

Tabulated data for the MnHCF compound calculated with the r^{2}SCAN functional.

Table S23: Structural properties of the manganese analogue Prussian Yellow (PY), Prussian Blue (PB), cubic Prussian White (PW) and rhombohedral Prussian White (RPW) as calculated with the r^{2}SCAN functional.

Property	PY	PB	PW	RPW
Space group	$Fm\bar{3}m$ (225)	$Fm\bar{3}m$ (225)	$Fm\bar{3}m$ (225)	$R\bar{3}$ (148)
a, b [Å]	10.003	10.168	10.515	6.402
c [Å]	10.525	–	–	19.162
V [Å^3]	1053.18	1051.14	1162.59	680.23
d(Fe_{ls}^{2+}-C) [Å]	1.895	1.878	1.875	1.871
d(C-N) [Å]	1.164	1.171	1.174	1.177
d(Fe_{hs}^{2+}-N) [Å]	2.117	2.036	2.208	2.217
α(Fe_{ls}^{2+}-C-N) [°]	180	180	180	172.4
α(Fe_{hs}^{2+}-N-C) [°]	180	180	180	137.4
α(C-Fe_{ls}^{2+}-C) [°]	90	90	90	87.4/92.6
α(N-Fe_{hs}^{2+}-N) [°]	90	90	90	91.8/88.2

Table S24: Electronic properties of the manganese analogue Prussian Yellow (PY), Prussian Blue (PB), cubic Prussian White (PW) and rhombohedral Prussian White (RPW) as calculated with the r^{2}SCAN functional.

Property	PY	PB	PW	RPW
VB_{Max} [eV]	–	–	-0.520	0.361
CB_{min} [eV]	–	–	-0.229	0.717
ΔE_g [eV]	cond.	cond.	0.291	0.356
$\mu_{Fe(II)\text{-}C}$ [μ_B]	1.009	0.136	0.059	0.059
$\mu_{Fe(II)\text{-}N}$ [μ_B]	3.603	3.613	4.512	4.488

5.5 PBE0 functional

Tabulated data for the MnHCF compound calculated with the PBE0 functional.

Table S25: Structural properties of the manganese analogue Prussian Yellow (PY), Prussian Blue (PB), cubic Prussian White (PW) and rhombohedral Prussian White (RPW) as calculated with the PBE0 functional.

Property	PY	PB	PW	RPW
Space group	$Fm\bar{3}m$ (225)	$Fm\bar{3}m$ (225)	$Fm\bar{3}m$ (225)	$R\bar{3}$ (148)
a, b [Å]	10.030	10.545	10.549	6.556
c [Å]	10.576	–	–	18.714
V [Å^3]	1063.89	1172.72	1173.82	696.66
d(Fe_{ls}^{2+}-C) [Å]	1.914	1.915	1.884	1.878
d(C-N) [Å]	1.156	1.160	1.167	1.171
d(Fe_{hs}^{2+}-N) [Å]	2.126	2.200	2.223	2.236
α(Fe_{ls}^{2+}-C-N) [°]	180	180	180	175.0
α(Fe_{hs}^{2+}-N-C) [°]	180	180	180	137.3
α(C-Fe_{ls}^{2+}-C) [°]	90	90	90	88.6/91.4
α(N-Fe_{hs}^{2+}-N) [°]	90	90	90	92.2/87.8

Table S26: Electronic properties of the manganese analogue Prussian Yellow (PY), Prussian Blue (PB), cubic Prussian White (PW) and rhombohedral Prussian White (RPW) as calculated with the PBE0 functional.

Property	PY	PB	PW	RPW
VB_{Max} [eV]	-3.439	–	–	–
CB_{min} [eV]	-0.440	–	–	–
ΔE_g [eV]	2.999	cond.	cond.	cond.
$\mu_{Fe(II)\text{-}C}$ [μ_B]	0.990	-0.944	0.039	0.039
$\mu_{Fe(II)\text{-}N}$ [μ_B]	3.713	4.568	4.579	4.570

5.6 HSE06 functional

Tabulated data for the MnHCF compound calculated with the HSE06 functional.

Table S27: Structural properties of the manganese analogue Prussian Yellow (PY), Prussian Blue (PB), cubic Prussian White (PW) and rhombohedral Prussian White (RPW) as calculated with the HSE06 functional.

Property	PY	PB	PW	RPW
Space group	$Fm\bar{3}m$ (225)	$Fm\bar{3}m$ (225)	$Fm\bar{3}m$ (225)	$R\bar{3}$ (148)
a, b [Å]	10.033	10.591	10.552	6.711
c [Å]	10.565	–	–	17.843
V [Å^3]	1063.55	1187.85	1174.84	695.91
d(Fe_{ls}^{2+}-C) [Å]	1.913	1.914	1.884	1.871
d(C-N) [Å]	1.156	1.160	1.168	1.171
d(Fe_{hs}^{2+}-N) [Å]	2.124	2.224	2.224	2.232
α(Fe_{ls}^{2+}-C-N) [°]	180	180	180	175.4
α(Fe_{hs}^{2+}-N-C) [°]	180	180	180	134.7
α(C-Fe_{ls}^{2+}-C) [°]	90	90	90	88.4/91.6
α(N-Fe_{hs}^{2+}-N) [°]	90	90	90	92.6/87.4

Table S28: Electronic properties of the manganese analogue Prussian Yellow (PY), Prussian Blue (PB), cubic Prussian White (PW) and rhombohedral Prussian White (RPW) as calculated with the HSE06 functional.

Property	PY	PB	PW	RPW
VB_{Max} [eV]	–	-3.537	–	–
CB_{min} [eV]	–	-3.347	–	–
ΔE_g [eV]	cond.	0.190	cond.	cond.
$\mu_{Fe(II)\text{-}C}$ [μ_B]	0.993	-0.950	0.039	0.040
$\mu_{Fe(II)\text{-}N}$ [μ_B]	3.714	4.581	4.579	4.567

6 Site preference measurement in Prussian Blue materials

This section examines the sodium site preference between the 8c and 24d Wyckoff positions across various XC-functionals. The data, presented in Figure S4, show that sodium consistently prefers the 24d site, with relative energy differences in the range of 0.4 to 0.6 eV. This trend is stable across all XC-functionals, indicating that the 24d site is generally more favorable for sodium intercalation. Only a minor increase in site preference is observed as the material transitions from Prussian Blue to Prussian White. However, exceptions occur with the PBE+U functional, where fully sodiated FeHCF and half-sodiated MnHCF configurations display an anomalous increase in site preference of approximately 300%. These results are believed to arise from the same artificial stabilization effects discussed in the main manuscript.

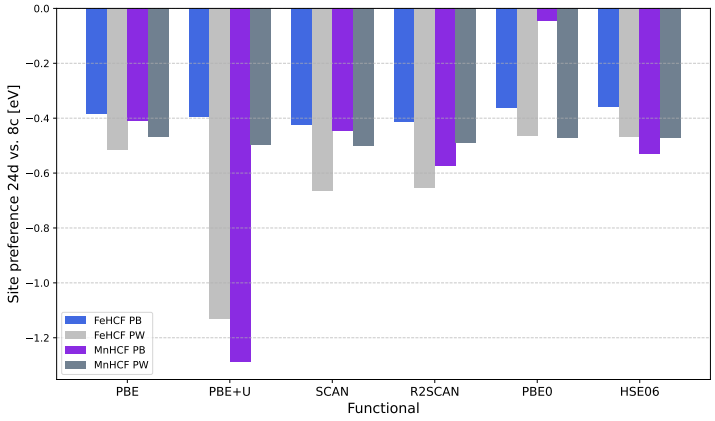

Figure S4: Relative stability of sodium intercalation into the 8c versus 24d Wyckoff positions in half- and fully sodiated FeHCF and MnHCF systems. Negative values denote a thermodynamic preference for the 24d site. Data for FeHCF are shown in blue (half-sodiated) and light grey (fully sodiated); MnHCF values are shown in purple (half-sodiated) and dark grey (fully sodiated).

7 Floating point data on migration barriers in FeHCF

Table S29: Relative energies [meV] along the ladder-like sodium migration in the high-vacancy limit of cubic Prussian Yellow.

Energy [meV]	PBE	PBE+U	SCAN	r^{2}SCAN	PBE0	HSE06
initial	0.0	0.0	0.0	0.0	0.0	0.0
TS1	83.8	0.0	264.4	56.7	58.9	58.6
mid	-1.4	0.0	-1.0	10.9	-7.1	-7.8
TS2	83.3	0.0	210.6	56.6	60.3	69.2
final	0.9	0.0	41.1	6.3	-3.9	-3.3

Table S30: Relative energies [meV] along the ladder-like sodium migration in the half-sodiated, cubic Prussian Blue.

Energy [meV]	PBE	PBE+U	SCAN	r^{2}SCAN	PBE0	HSE06
initial	0.0	0.0	0.0	0.0	0.0	0.0
TS1	108.3	135.4	0.0	128.7	110.5	33.2
mid	85.9	169.1	0.0	105.5	132.3	167.0
TS2	296.0	451.2	0.0	320.2	448.6	355.1
final	289.4	509.4	0.0	391.0	556.3	484.5

Table S31: Relative energies [meV] along the ladder-like sodium migration in the low-vacancy limit of cubic Prussian White.

Energy [meV]	PBE	PBE+U	SCAN	r^{2}SCAN	PBE0	HSE06
initial	0.0	0.0	0.0	0.0	0.0	0.0
TS1	38.1	87.7	0.0	56.7	165.4	0.0
mid	9.8	37.5	0.0	11.5	79.1	0.0
TS2	52.9	225.9	0.0	41.4	158.6	0.0
final	-1.1	91.7	0.0	5.3	2.9	0.0

Table S32: Relative energies [meV] along the sodium migration pathway in the low-vacancy limit for the rhombohedral modification of Prussian White.

Energy [meV]	PBE	PBE+U	SCAN	r^{2}SCAN	PBE0	HSE06
initial	0.0	0.0	0.0	0.0	0.0	0.0
TS1	363.4	417.7	267.0	277.2	503.7	0.0
final	29.3	-18.1	15.0	1.0	-0.4	0.0

Table S33: Relative energies [meV] along the sodium migration pathway across the Wyckoff 8c site in the high-vacancy limit of cubic Prussian Yellow.

Energy [meV]	PBE	PBE+U	SCAN	r^{2}SCAN	PBE0	HSE06
initial	0.0	0.0	0.0	0.0	0.0	0.0
TS1	329.6	214.0	481.5	0.0	276.6	275.7
final	0.9	-5.8	41.1	0.0	-3.9	-3.3

Table S34: Relative energies [meV] along the sodium migration pathway across the Wyckoff 8c site in the half-sodiated, cubic Prussian Blue.

Energy [meV]	PBE	PBE+U	SCAN	r^{2}SCAN	PBE0	HSE06
initial	0.0	0.0	0.0	0.0	0.0	0.0
TS1	348.0	353.4	519.9	346.5	424.6	381.8
final	289.4	509.4	529.8	391.0	556.3	484.5

Table S35: Relative energies [meV] along the sodium migration pathway across the Wyckoff 8c site in the low-vacancy limit of cubic Prussian White.

Energy [meV]	PBE	PBE+U	SCAN	r^{2}SCAN	PBE0	HSE06
initial	0.0	0.0	0.0	0.0	0.0	0.0
TS1	322.4	534.8	349.2	425.1	264.6	456.8
final	-1.1	92.8	-46.4	5.3	2.9	1.3

References

[1] X. Wu, W. Deng, J. Qian, Y. Cao, X. Ai, H. Yang, *J. Mater. Chem. A* **2013**, *1*, 10130–10134.